The International Journal of Advanced Manufacturing Technology
https://doi.org/10.1007/s00170-026-18191-6

ORIGINAL ARTICLE

Impact of abrasive jet machining on the fatigue behaviour of corrosion-exposed UNS A97075 alloy

Sergio Martín-Béjar[1] · Ignacio Repiso López[1] · Manuel Herrera Fernández[1] · Francisco Javier Trujillo Vilches[1] · Lorenzo Sevilla Hurtado[1]

Received: 4 October 2025 / Accepted: 18 April 2026

Abstract
Surface conditions are a decisive factor in the fatigue performance of aeronautical components, particularly for alloys highly susceptible to corrosion, such as UNS A97075. This study investigates the combined influence of machining parameters, corrosion, and Abrasive Jet Machining on the geometric accuracy, surface roughness, and fatigue behaviour of rotary-bending specimens. Two cutting conditions were applied, followed by controlled sequences of corrosion and Abrasive Jet Machining to evaluate their synergistic effects. The results show that machining under more severe conditions increased roughness and form deviations owing to higher cutting forces, vibration and thermal loading. However, the sequence of post-machining operations exerted a far greater impact on surface conditions and fatigue life than machining parameters alone. When Abrasive Jet Machining was applied after corrosion, roundness and cylindricity were partially restored, roughness was stabilised, and fatigue life was significantly extended. Conversely, Abrasive Jet Machining performed before corrosion amplified pitting, produced severe geometric distortions, and reduced fatigue life by more than 50%. These findings demonstrate the dual role of Abrasive Jet Machining as either a restorative or detrimental treatment depending on process order, providing clear guidance for the optimisation of manufacturing and maintenance strategies in aerospace aluminium alloys exposed to corrosive environments.

Keywords Abrasive jet machining · Fatigue behaviour · Corrosion · Dry turning · UNS A97075

1 Introduction

The aerospace industry is one of the most strategic and technologically demanding sectors worldwide, characterised by strict safety, reliability, and performance requirements [1]. Modern aircraft design and operation require materials that can withstand extremely severe service conditions, where structural weight reduction, high mechanical strength, and durability under cyclic loading or aggressive environments are decisive factors [2, 3]. Therefore, material selection for aeronautical applications is based not only on mechanical performance but also on fuel efficiency, reduced operational costs, and flight safety.

Aluminium alloys have played a special role in the aeronautical industry, progressively replacing heavier metals due to their outstanding strength-to-weight ratio. These alloys are distinguished by their low density, good formability, high specific strength, and advantageous balance between toughness and corrosion resistance, making them an excellent material for aircraft structures [4, 5]. Despite the increasing use of advanced composite materials, such as carbon fibre reinforced polymers (CFRPs) [6], aluminium alloys remain essential in multiple aircraft components due to their versatility, proven reliability, and maturity of associated manufacturing technologies [7].

Within the wide range of aluminium alloys, the UNS A97075 alloy is particularly relevant for aerospace applications [8]. This precipitation-hardened, zinc-rich alloy exhibits one of the highest strength levels among commercial aluminium grades, with yield strengths exceeding 500 MPa [9]. Owing to this exceptional combination of high strength and low weight, this alloy is commonly used in structural elements, such as wing spars and ribs, landing gear

✉ Sergio Martín-Béjar
smartinb@uma.es

[1] Department of Civil, Material and Manufacturing Engineering, EII, University of Malaga, C/Dr, Ortiz Ramos s/n, Malaga E- 29071, Spain

Published online: 30 April 2026

components, fuselage frames, and precision machined parts, subjected to severe mechanical stresses [10, 11]. Beyond civil aviation, this alloy also finds applications in the aerospace and defence industries, including helicopter components, missile structures, and military vehicles, underlining its strategic relevance [11].

Surface integrity is a critical attribute in aerospace manufacturing, where the highest quality requirements must be met to ensure the safety and reliability of structural components [12, 13]. Even minor surface imperfections in this sector can lead to premature failures under high cyclic stresses and aggressive environments. Therefore, the control and characterisation of surface integrity have become essential aspects of aeronautical design, manufacturing, and maintenance.

The term surface integrity refers to the macrogeometric, microgeometric, and physicochemical properties that define a material's surface condition after manufacturing or postprocessing [14]. From the macrogeometric perspective, it encompasses form deviations, such as roundness, straightness, and cylindricity, which are decisive for the dimensional and functional accuracy of aerospace components [15]. On the microgeometric level, surface roughness plays a key role, as it governs stress concentration phenomena that strongly affect fatigue crack nucleation [16, 17]. Finally, from the physicochemical standpoint, surface integrity also includes properties such as corrosion resistance and fatigue behaviour, which determine the durability of components under combined environmental and mechanical loading [18].

In aerospace applications, the interaction between these macrogeometric, microgeometric, and physicochemical aspects of surface integrity directly influences the structural performance and fatigue life of aluminium alloys, such as UNS A97075 [16]. Therefore, understanding and controlling these parameters is essential for optimising manufacturing strategies and ensuring the long-term reliability of aircraft structures. In this context, manufacturing process selection and parameter definition are central to controlling surface integrity in aerospace aluminium alloys.

Machining operations are a fundamental step in the manufacturing of aeronautical structural components, as they enable the achievement of the strict dimensional tolerances and geometric accuracy required in the aerospace sector. Aluminium alloys, such as UNS A97075, are widely used in these applications owing to their high specific strength and excellent machinability, which facilitates the production of complex and high-precision parts [5, 19].

However, in recent years, increasing environmental concerns have driven a progressive shift towards dry machining, aiming to reduce the use of cutting fluids [20]. Conventional cutting fluids, although beneficial in reducing tool wear and improving surface finish, pose serious environmental challenges because of their toxicity, disposal requirements, and impact on operator health [21]. Therefore, their elimination represents an important step towards more sustainable and eco-efficient manufacturing processes.

Despite the inherently good machinability of aluminium alloys, dry machining imposes more severe cutting conditions than conventional lubrication-assisted operations. The absence of cutting fluids results in higher cutting zone temperatures, increased cutting forces, and greater tool–workpiece interaction [22]. Consequently, the process becomes more aggressive and may deteriorate the surface integrity through increased roughness, higher form deviations, and the potential induction of residual stresses. As a result, while dry machining offers clear environmental and economic advantages, it also poses significant challenges in terms of maintaining the required surface quality for aerospace components [23].

Abrasive Jet Machining (AJM) is a nonconventional postprocessing operation that employs a high-velocity stream of abrasive particles to erode a material's surface. In the aerospace industry, this technique has been increasingly considered a complementary process to conventional machining, particularly for components manufactured from aluminium alloys. Its primary purpose is to improve surface conditions after initial machining by removing irregularities, reducing surface defects, and enhancing overall dimensional accuracy [24, 25].

AJM offers several advantages in the machining of aluminium alloys. The process enables surface roughness modification and eliminates machining-induced marks or shallow corrosion pits, thereby improving the surface topography homogeneity [26]. Additionally, AJM avoids issues related to tool wear and cutting forces because it is a noncontact process, making it suitable for finishing delicate or geometrically complex aerospace components [27]. Surface bombardment by abrasive particles may induce beneficial compressive residual stresses in the surface layer, which can improve fatigue resistance [28, 29].

Nevertheless, AJM must be carefully controlled, as the same abrasive action that removes defects may also introduce new surface irregularities or microcracks, potentially compromising the material's mechanical performance [30]. Understanding the balance between the beneficial and detrimental effects of AJM is critical for its successful application in aerospace manufacturing and maintenance.

Although aluminium alloys generally show good corrosion resistance, UNS A97075 exhibits lower corrosion resistance due to its zinc-rich composition. This alloy is particularly susceptible to localised corrosion phenomena, including pitting corrosion and stress corrosion cracking, which are intensified in chloride-containing environments

such as saline atmospheres [31]. These types of degradation act as preferential sites for the initiation of fatigue cracks, reducing the service life of aerospace components exposed to aggressive conditions.

Exposure to humid or marine environments accelerates the onset of pitting in aircraft structures, creating surface cavities that act as severe stress concentrators under cyclic loading. Moreover, the combination of mechanical stress and corrosive attack promotes stress corrosion cracking, leading to premature failure even at stress levels well below the material's nominal yield strength [32]. These effects are especially critical in structural elements, such as fuselage frames, wing components, and landing gear assemblies, which are routinely exposed to fluctuating mechanical loads and corrosive agents during service.

The interaction between machining-induced surface features and corrosion further complicates this scenario. Machining marks, residual stresses, or geometric deviations can intensify localised corrosion, creating conditions favourable to early crack nucleation [33, 34]. Therefore, understanding how corrosion alters the surface integrity of UNS A97075 and how postprocessing operations such as AJM may mitigate or amplify these effects is critical for ensuring the long-term reliability of aerospace components.

These facts make fatigue behaviour one of the most critical mechanical properties in the aerospace industry, as it directly affects the safety and reliability of aircraft structures. Aerospace components are continuously subjected to cyclic loading during service. If not properly controlled, the progressive initiation and propagation of fatigue cracks can lead to catastrophic failures. Therefore, fatigue resistance analysis and improvement represent a fundamental requirement in aeronautical design, manufacturing, and maintenance.

The fatigue behaviour of aluminium alloys, such as UNS A97075, is strongly influenced by surface integrity. Surface roughness plays a decisive role in introducing stress concentrators that facilitate crack nucleation under cyclic stresses. Even small increases in roughness may drastically reduce the number of cycles to failure, highlighting the need for strict surface quality control [16, 35].

Manufacturing and postprocessing operations also exert a direct influence on fatigue life. The machining conditions determine the initial roughness, which may introduce residual stresses or geometric deviations that modify fatigue performance [36]. Corrosion accelerates the initiation of cracks by generating pits and surface defects that act as critical stress raisers [37]. Similarly, Abrasive Jet Machining, while capable of reducing certain machining or corrosion-induced defects, can also introduce new surface irregularities or microcracks if not properly controlled [38]. Thus, the combined effects of machining, corrosion, and AJM have a synergistic impact on fatigue resistance, underscoring the importance of systematically studying their interactions.

Recent evidence from particle impact surface treatments supports the notion that fatigue performance can be governed by impact craters and the population of local surface defects, rather than by average roughness alone. Dai et al. [39] showed that grit blasting can shift the initiation of fatigue cracks to impact craters and that fatigue life is strongly dependent on process parameters such as abrasive size and pressure. In a related context, Bakir et al. [40] found that cold spray repair on UNS A97075 can recover fatigue performance, while crack initiation may localise at the substrate deposit interface where particle impact leaves crater-like features. Furthermore, Sarkar et al. [41] demonstrated that the fatigue benefit of glass bead blasting is markedly reduced when the treatment is applied after corrosion because corrosion-related defects remain dominant sites for crack initiation. These recent findings highlight the dual role of particle-based postprocessing and reinforce the need for dedicated studies that account for corrosion exposure and process sequence when assessing fatigue behaviour.

The initial surface state is set by machining conditions and can affect fatigue behaviour through roughness, residual stresses, and geometric deviations. Chloride-induced pitting reduces fatigue life by creating surface defects that promote crack initiation. In addition, depending on the severity of the process, particle-impact treatments can either improve or worsen fatigue performance, and crack initiation may shift from machining marks to impact craters or defects caused by corrosion. However, most studies consider these factors separately and do not clarify how the combination of corrosion exposure and particle-based treatments changes fatigue response. The combined effect of machining, corrosion, and abrasive particle treatments in UNS A97075 remains unclear, particularly when the processes are applied in different sequences.

In aerospace manufacturing and maintenance, abrasive particle processes, such as AJM, can be applied after machining to modify or improve surface conditions before service. In this situation, the surface state prior to environmental exposure differs from that of a conventionally machined component, and the subsequent corrosion behaviour may evolve in a different manner due to the altered topography and defect distribution. At the same time, abrasive processes may also be used on components that have already experienced corrosion to remove oxide layers or superficial damage. In such cases, the treatment modifies a surface that already contains corrosion pits and defects, which can alter the material's geometric integrity and fatigue response. Despite these practical scenarios, systematic evidence clarifying how the application of AJM before or after corrosion

affects surface integrity and fatigue performance in UNS A97075 is still limited.

The present study addresses this gap through a controlled experimental framework in which two contrasted dry turning conditions are combined with two alternative sequences involving corrosion and Abrasive Jet Machining. The novelty of the work lies in isolating the effect of process sequence under controlled turning conditions and in relating that sequence directly to surface roughness, macrogeometric deviations, and rotary bending fatigue behaviour in UNS A97075. Standardised measurements of roughness, form deviations, and fatigue performance are integrated to determine whether AJM acts as a harmful treatment when applied before corrosion or as a restorative treatment when applied afterwards. In this way, the study provides both mechanistic interpretation and practical guidance for manufacturing and maintenance strategies in aerospace aluminium components exposed to corrosive environments.

2 Methodology

To investigate the effects of machining, corrosion and AJM on the fatigue behaviour of UNS A97075 aluminium alloy, a systematic experimental procedure was followed. The specimen dimensions were designed to meet the requirements for rotary bending fatigue tests, as specified in ISO 1143:2010 [42] (Fig. 1a). Among the various geometries proposed by the standard for fatigue test specimens, the parallel specimen was chosen because of its ease of machining. This geometry requires a lower applied load while producing a higher bending moment in the expected fracture zone.

The machining process was performed using a CNC turning centre, model EMCO TURN E45 (Fig. 1b). A rhombic uncoated WC-Co tool (ISO DCMT 11T308-14 IC20) was used with a neutral tool holder configuration during turning. A new cutting edge was used for each test to ensure that the initial conditions were consistent. The main cutting-edge angle was set to 62.5° to ensure proper machining of the calibrated zone, which corresponds to the test section thickness. The machining operation was carried out under dry conditions for environmental reasons.

Two combinations of cutting speed (v_c) and feed (f) values were used during machining: low cutting parameter values (v_c = 40 m/min, f = 0.05 mm/rev) and high cutting parameters (v_c = 80 m/min, f = 0.20 mm/rev). Although higher cutting speeds are feasible for aluminium alloys, the selected v_c values are appropriate for the machining of hybrid structures involving CFRP, which are common in the aerospace industry [43]. Therefore, this range allowed the evaluation of how moderate versus severe cutting conditions generate two clearly contrasting initial surface integrity states before corrosion and AJM. The two-level design kept the experimental matrix manageable and enabled a controlled comparison of the post-processing sequences.

Two additional operations were performed on the specimens after machining to modify their surface conditions. One operation involved Abrasive Jet Machining, in which particles were projected onto the specimen surface (Fig. 2a). This operation was performed at a constant pressure of 8 bar, with a fixed stand-off distance from the workpiece surface, and glass beads were used as the abrasive particles. These parameters were chosen to ensure a uniform surface

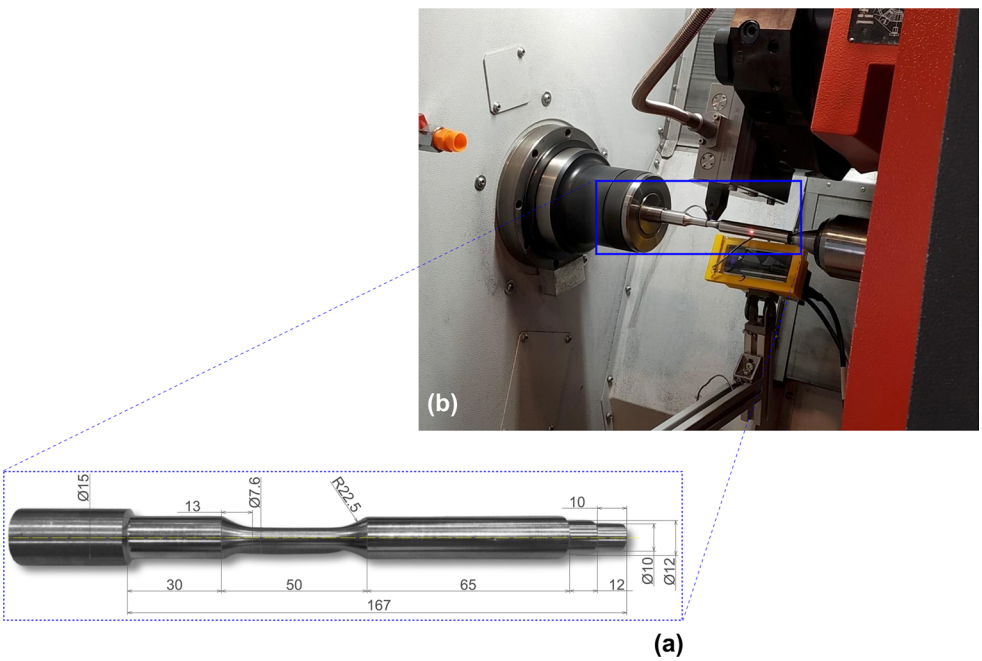

Fig. 1 (**a**) Specimen geometry; (**b**) machining centre

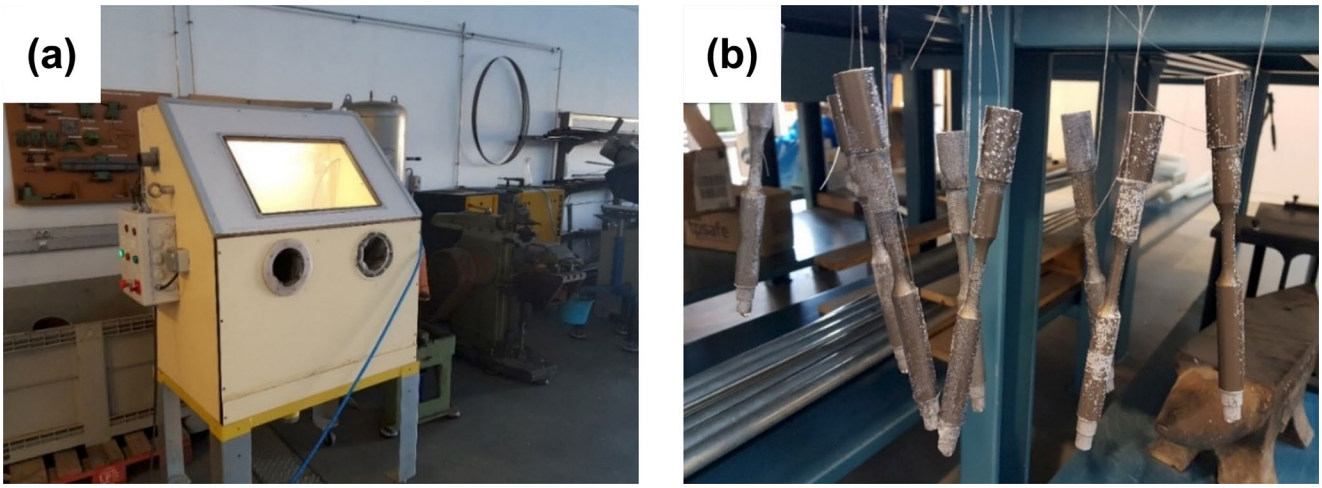

Fig. 2 (**a**) AJM equipment; (**b**) corrosion tests

modification while avoiding excessive material removal, in line with previous studies on aluminium alloys [26, 44].

The second operation consisted of exposing the specimens to corrosion by immersion in a saline solution (Fig. 2b). This treatment was carried out in a 3.5% NaCl solution for three days in order to modify the surface state obtained after machining. This condition promotes chloride-induced pitting in a controlled and accelerated manner. Pitting is a common and highly relevant degradation mechanism in UNS A97075 aluminium alloy used in aircraft structures exposed to saline contamination, and generating measurable pitting in a repeatable way is essential for a reliable comparison of the post-processing effects.

A water circulation pump was used to ensure uniform corrosion across the entire surface and maintain a consistent NaCl concentration throughout the solution. Additionally, the solution temperature was checked every 24 h to ensure process stability. After immersion, each specimen was cleaned to remove any residual NaCl deposits from the surface.

These operations were carried out in different sequences to determine their effects on the surface conditions of the machined specimens. Considering the process order makes it possible to determine whether AJM can restore surface integrity after corrosion damage or whether applying it beforehand intensifies the adverse effects of subsequent corrosion. Table 1 summarises the operations performed and their corresponding sequences.

Table 1 Order of operations during the experimental phase

1 st operation	2nd operation	3rd operation
Turning (v_c = 40 m/min; f=0.05 mm/rev)	AJM	Corrosion
Turning (v_c = 40 m/min; f=0.05 mm/rev)	Corrosion	AJM
Turning (v_c = 80 m/min; f=0.20 mm/rev)	AJM	Corrosion
Turning (v_c = 80 m/min; f=0.20 mm/rev)	Corrosion	AJM

The surface roughness of each specimen was measured after each operation (Fig. 3). Measurements were taken after machining, after the corrosion process, and after the AJM operation. The arithmetic mean roughness (*Ra*) and the mean profile height (*Rz*) were characterised using a Mitutoyo SJ-210 roughness tester. The measurements were performed over a sampling length of 0.8 mm (*lc*), taking a total of five samples and applying a Gaussian filter to eliminate shape and waviness components, in compliance with the requirements of ISO 4288:1998 [45] (Fig. 3a).

The form deviations were assessed in the calibrated section of the fatigue specimens, as this region contains the highest bending stresses during rotary bending and constitutes the most likely zone for fatigue fracture. The accurate characterisation of geometric deviations in this area is essential because imperfections, such as roundness or straightness errors, can act as stress concentrators and directly influence the initiation and propagation of fatigue cracks [46].

Measurements were carried out using a RONDCOM NEX form measuring instrument (Fig. 3b), which provides high-resolution profiling of rotationally symmetric parts. All form measurements were performed following the same mounting and alignment procedure for all specimens and conditions, and end-effects were avoided by limiting the evaluation to the calibrated section. The acquisition of multiple profiles was adopted to minimise sensitivity to local outliers and improve the representativeness of the measured form errors across the gauge length.

Up to six roundness profiles were acquired on parallel cross-sections within the calibrated section, with an axial spacing of 4 mm between consecutive sections. This sampling strategy ensured a representative description of the roundness error throughout the gauge length. The roundness deviation was evaluated using the least-squares circle method, as specified in ISO 12181-1:2011 [47], which

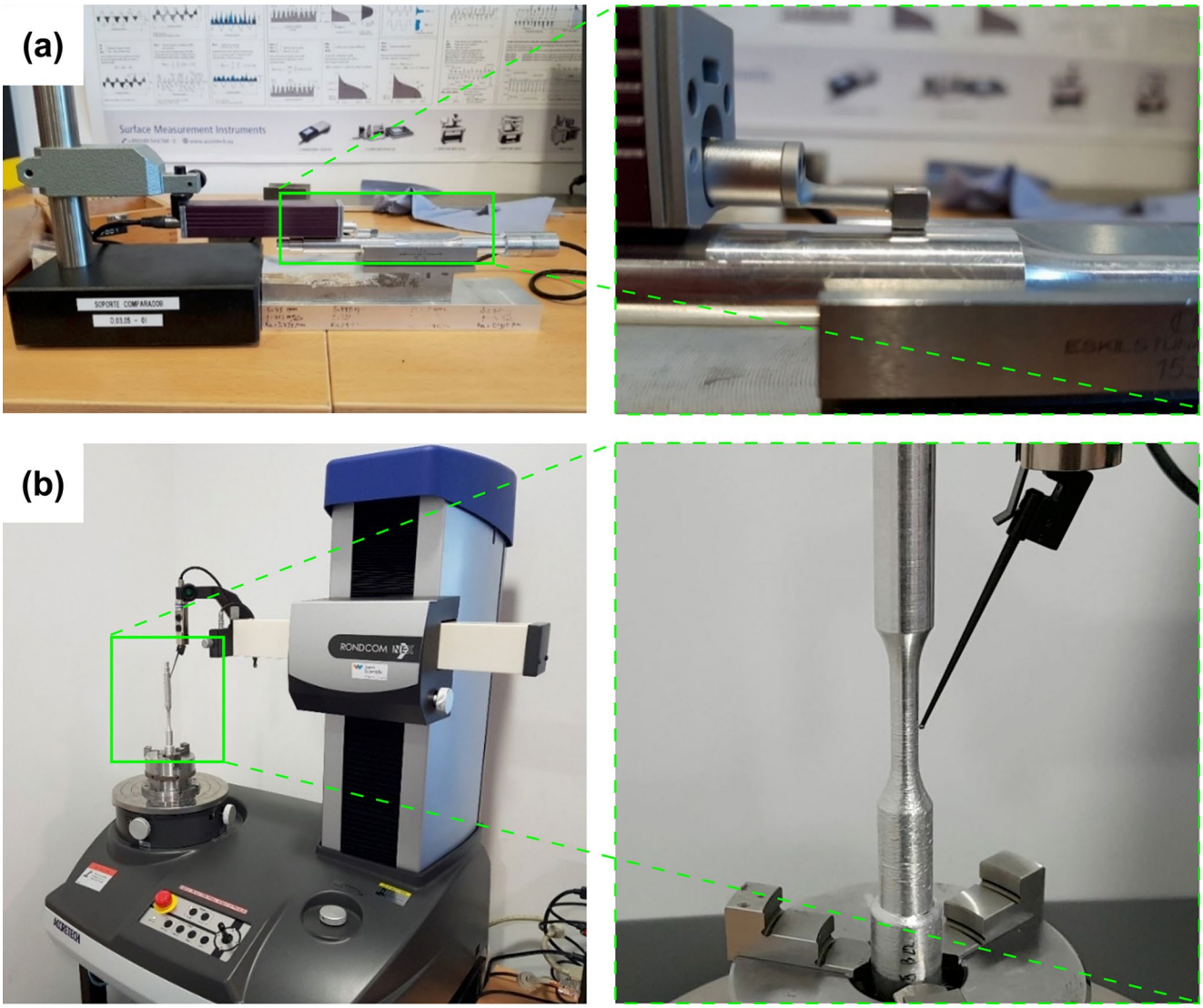

Fig. 3 (**a**) Surface roughness measurement; (**b**) measurement of form deviations

determines the radial difference between the measured profile and the reference circle that minimises the sum of squared deviations.

The straightness was subsequently measured along the surface generatrix of the calibrated section to capture potential axial distortions. Four measurements were performed over a length of 15 mm, each separated by 90° around the circumference, thereby covering the entire perimeter of the specimen. This approach enabled the detection of directional variability in the straightness error. The evaluation followed the procedures established in ISO 12780-1:2011 [48], which defines the least-squares line as the reference for straightness assessment.

Rotary bending fatigue tests (Fig. 4) were carried out to evaluate the influence of machining, corrosion, and AJM on the fatigue behaviour of UNS A97075 aluminium alloy. The tests were performed using a rotary bending machine developed at the University of Málaga, following ISO 1143:2010 specifications for metallic materials. The specimens were subjected to a fully reversed loading condition (stress ratio $R = -1$), which is representative of high-cycle fatigue in aerospace applications.

A single load of 9 kgf was applied at the free end of each specimen, corresponding to a nominal stress amplitude of approximately 230 MPa in the calibrated section, where fracture was expected to occur. This stress amplitude was deliberately selected to ensure that surface integrity remained a relevant driver of fatigue performance, particularly in the presence of corrosion-related surface defects. At higher stress amplitudes, crack initiation may occur more rapidly, reducing the sensitivity of fatigue life to differences in surface condition and partially masking the influence of the post-processing operations.

During testing, the rotation frequency was set to 50 Hz to ensure a balance between testing efficiency and

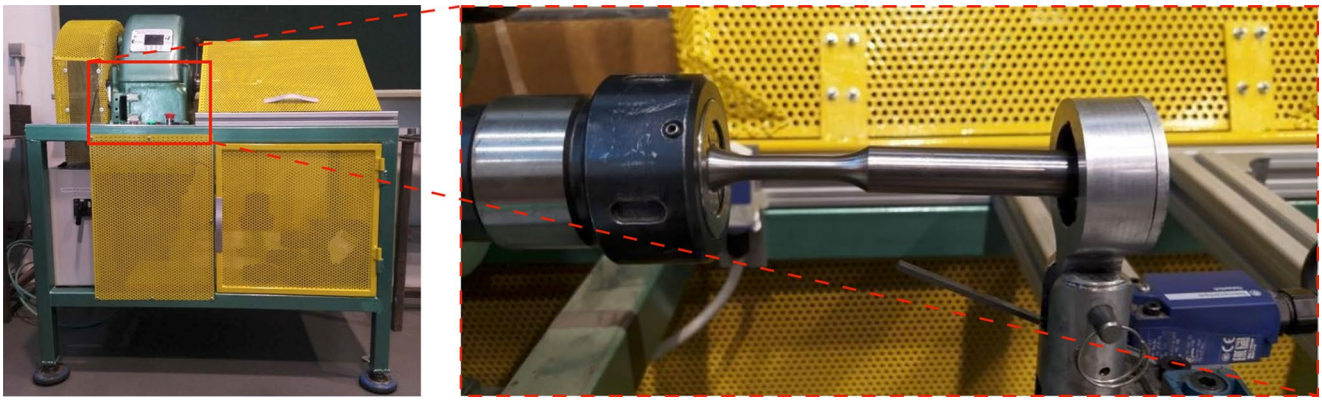

Fig. 4 Rotary bending fatigue test bench

minimisation of thermal effects. The fatigue life (N) was defined as the number of cycles to complete the fracture of the specimen.

Four specimens were tested for each manufacturing condition and process sequence described in Table 1 to guarantee statistical reliability of the results. This replication enabled the calculation of mean values and standard deviations, ensuring a 95% confidence level in the fatigue life data obtained according to ISO 12107:2012.

Notably, this experimental procedure was structured to isolate the effect of the process sequence under two contrasted initial machining conditions. The turning parameters were selected to generate two distinct initial surface integrity states, while the corrosion exposure and AJM settings were kept constant across all specimens. This design enables a direct comparison between the two operation sequences and supports the attribution of the observed differences in roughness, form deviations, and fatigue life to process order within the investigated conditions.

3 Results

3.1 Analysis of surface roughness

Figure 5 shows the mean values of the arithmetic mean roughness (Ra) after each manufacturing operation carried out on the fatigue test specimens of UNS A97075 aluminium alloy: turning operation, corrosion under saline solution, and AJM.

After turning, the specimens machined under the lower cutting parameters showed lower Ra values than those machined under the more aggressive condition. This difference can be attributed to the interplay between the cutting conditions and the removal mechanism. A lower feed rate (0.05 mm/rev) reduces the depth of the grooves formed by the cutting tool, resulting in a smoother surface finish. Furthermore, the lower cutting speed minimises heat generation in the cutting zone, reducing tool adhesion wear (built-up edges, BUE), which can transfer irregular material deposits onto the surface and increase surface roughness.

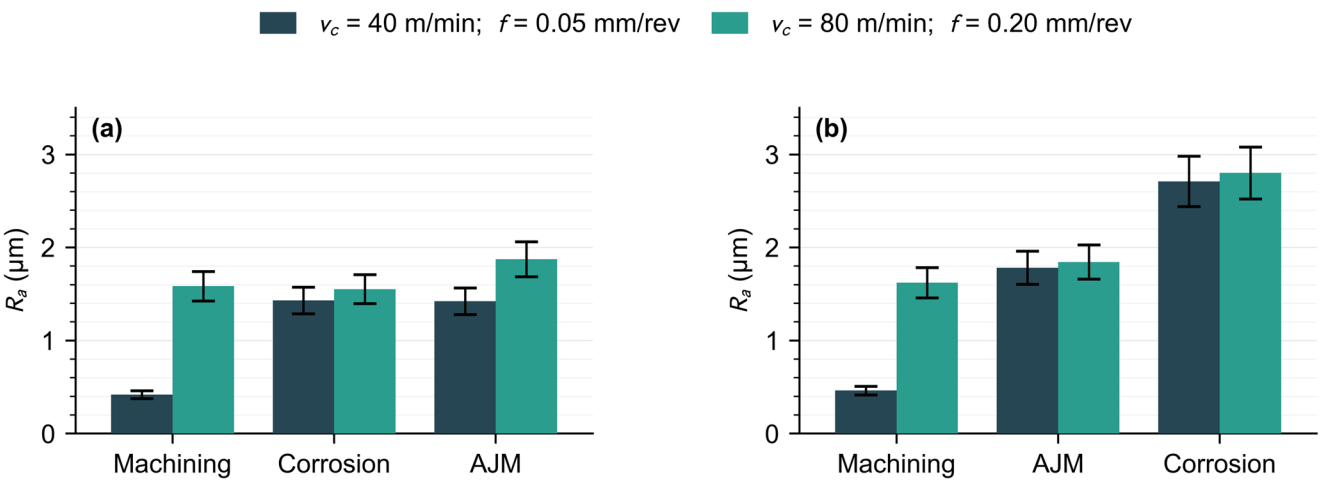

Fig. 5 Arithmetic mean roughness. (**a**) Corrosion before the AJM process; (**b**) AJM before corrosion

Aggressive machining conditions (80 m/min and 0.20 mm/rev) generate a rougher surface due to the combined effects of higher feed rates and elevated cutting speeds. The higher feed rate increases the spacing between successive tool passes, leaving deeper and more prominent machining marks. Simultaneously, the higher cutting speed increases heat accumulation in the cutting zone, promoting thermal softening of the material and potentially leading to localised smearing or tearing of the surface. Furthermore, higher cutting conditions increase vibrations and dynamic forces, resulting in irregularities in the machined surface. These combined factors explain the higher *Ra* values observed for specimens machined under high cutting parameter values.

In the second stage, specimen exposure to a corrosive environment through immersion in a saline solution increases *Ra* (Fig. 5a). Under such conditions, the predominant type of corrosion observed in UNS A97075 is pitting corrosion, which creates irregularities and localised depressions on the surface, increasing *Ra*. The lack of a significant increase in *Ra* after corrosion in specimens initially machined under higher cutting parameters may be attributed to the high initial surface roughness, which already features deep grooves and pronounced irregularities. The corrosion process tends to act within these existing defects, locally intensifying them without introducing substantial new irregularities that would further increase *Ra*. This saturation effect contrasts with specimens machined under lower cutting parameters, where the initially smoother surface allows the corrosion to create more noticeable deviations, leading to a greater increase in *Ra*.

After corrosion, the AJM process introduces a further increase in surface roughness, with a more pronounced effect on specimens machined under aggressive parameters. This surface already contains deeper grooves and irregularities resulting from machining and corrosion. These features amplify the impact of abrasive particles, as they preferentially erode areas of high stress concentration, creating deeper pits and enhancing roughness. In addition, the irregular surface topology increases the probability of abrasive particle scattering, resulting in inconsistent material removal and further amplifying *Ra*. Conversely, specimens machined under lower cutting parameters exhibit a smoother initial surface, which allows the abrasive particles to act more uniformly, resulting in a non-significant change in *Ra*.

Figure 5b shows the evolution of Ra when AJM was applied before exposure to the saline solution. After AJM, *Ra* increased under both machining conditions and reached very similar values in the two groups of specimens. This behaviour can be attributed to the AJM conditions, which generated roughness levels higher than those produced by turning alone. The high-velocity abrasive particles created new irregularities, such as microcracks, peaks and valleys, that dominated the surface profile and largely masked the influence of the initial cutting conditions.

Subsequent exposure to the corrosive environment after AJM produced a marked increase in Ra because corrosion acted on a surface that already contained numerous irregularities and stress concentrators created by the abrasive process. These features facilitated the nucleation and growth of localised corrosion, mainly pitting, thereby promoting a stronger increase in roughness during the final stage. Under this sequence, the influence of the initial cutting conditions on the final *Ra* became negligible because the surface state was dominated by AJM and the subsequent corrosion attack.

The final *Ra* is substantially higher when corrosion is performed after AJM than when AJM is performed after corrosion. For the low cutting parameter condition, the final *Ra* increases from 1.42 μm when corrosion is performed before AJM to 2.71 μm when corrosion is performed after AJM, corresponding to an increase of 90.7%. Under the high cutting parameter condition, the final *Ra* increases from 1.87 μm to 2.80 μm, corresponding to an increase of 49.4%. Therefore, comparing the two sequences revealed the significant influence of the process order on the surface roughness evolution. In the first scenario, where corrosion was applied before AJM, the increase in roughness caused by corrosion was partially mitigated during the subsequent abrasive process. The AJM removed some defects caused by pitting, partially levelling the surface and resulting in lower final *Ra* values. In contrast, in the second scenario, where AJM was applied before corrosion, the abrasive process amplified the corrosion effects. The irregularities and stress concentrators created during AJM facilitated the nucleation and progression of localised corrosion, leading to a greater increase in *Ra* during the final stage.

The evolution of *Rz* in the two process sequences, corrosion followed by AJM (Fig. 6a) and AJM followed by corrosion (Fig. 6b), was similar to that observed for *Ra*, showing that *Rz* was also highly sensitive to process order. A key difference, however, lay in the magnitude of the changes, particularly after the first operation applied after machining. At this stage, the increase in *Rz* was much more pronounced than that in *Ra*, regardless of whether corrosion or AJM was applied first. This is consistent with the nature of *Rz*, which reflects the distance between the highest peak and the deepest valley within the evaluation length and is therefore more sensitive to pronounced topographical features such as corrosion pits and particle-impact marks.

In the second stage, the magnitude of the *Rz* increase depends strongly on the order of the processes. In the case where corrosion follows AJM, the roughened surface created by the abrasive process contains numerous irregularities that act as nucleation sites for pitting during the

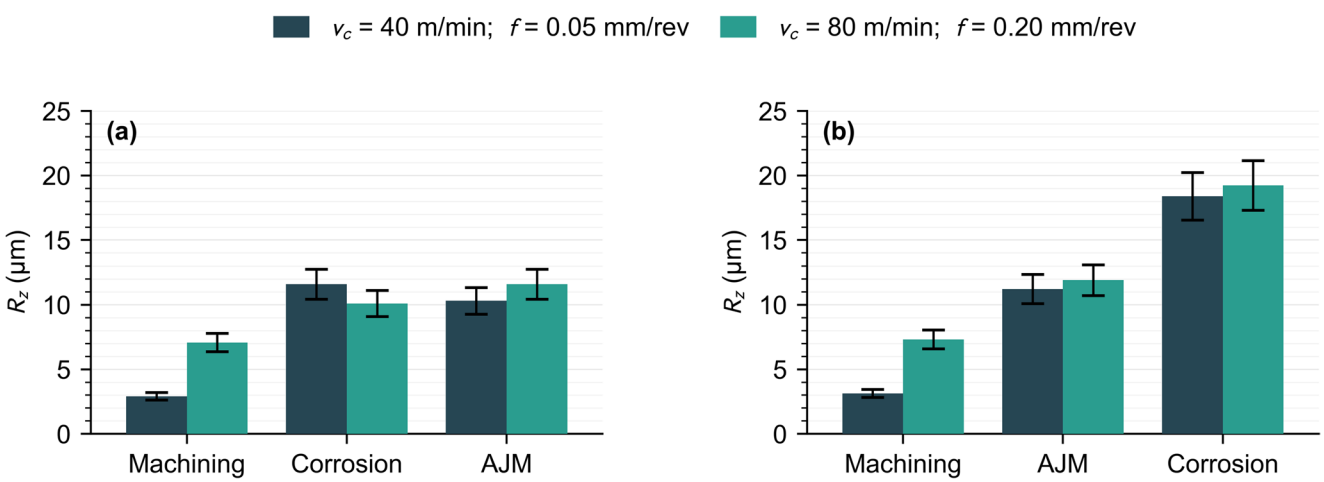

Fig. 6 The mean profile height. (**a**) Corrosion before the AJM process; (**b**) AJM before the corrosion process

corrosion process. These previous features intensify the corrosive attack, leading to a significant rise in *Rz*, which is greater than the increase observed when the first process is corrosion. In contrast, when AJM follows corrosion, the abrasive process partially removes the defects introduced during pitting, thereby limiting the extent to which *Rz* increases. According to this analysis, it responds similarly to *Ra* regarding the sensitivity to process order, but with notable differences in magnitude, especially during the first operation after machining.

The same trend was observed for the final *Rz* values, further demonstrating the sequencing effect. Under the low cutting parameter condition, the final *Rz* increases from 10.32 µm (corrosion before AJM) to 18.39 µm (corrosion after AJM), corresponding to an increase of 78.3%. Under the high cutting-parameter condition, the final *Rz* increases from 11.60 µm to 19.23 µm, corresponding to an increase of 65.7%. Therefore, the sequencing of corrosion and AJM leads to substantially larger percentage changes in the final *Rz* than those associated with changing the turning parameters within a given sequence, consistent with the trend observed for *Ra*.

Recent literature provides reference ranges for *Ra* and *Rz* that are consistent with the magnitudes measured in this study and supports the interpretation of the observed trends. Zdravkovic et al. [49] documented that P180 sanding on aluminium surfaces yields *Ra* values between 1.46 µm and 1.91 µm and *Rz* values between 8.65 µm and 12.33 µm, which is in line with the lower roughness levels obtained in this study. Moving from mechanical abrasion to particle-based surface treatments, substantially larger peak-to-valley amplitudes have been described in abrasive blasting [50], with values around *Ra* 4.25 µm and Rz 30.22 µm, exceeding the maxima measured in the present work and indicating that the AJM conditions applied here induce a moderate roughness increase when compared with strongly roughening blasting treatments. This difference is consistent with findings in grit blasting, where Dai et al. [39] showed that roughness increases with grit size and pressure and linked topography evolution to impact crater formation and surface scratching. In this context, the higher sensitivity of *Rz* observed in the present results is consistent with the surface states dominated by pits or particle impact features because extreme height parameters are particularly affected by localised cratering and scratching.

3.2 Analysis of form deviations

In this section, the form deviations in the calibrated region of the fatigue specimens are evaluated. Three geometrical deviations were selected in accordance with ISO standards: roundness (*RON*), straightness (*STR*), and cylindricity (*CYL*). These parameters provide complementary information on the fatigue test specimen's macrogeometric accuracy, which is relevant for fatigue crack initiation under rotary bending. Their analysis enables the assessment of how machining conditions and the sequencing of corrosion and AJM influence the global geometric integrity of the specimens and, therefore, their potential effect on fatigue behaviour.

For f = 0.05 mm/rev, the average *RON* remained relatively low, indicating good form accuracy in the calibrated section. In contrast, specimens machined under aggressive parameters (v_c = 80 m/min; f = 0.20 mm/rev) exhibited a significant increase in *RON*. This behaviour is consistent with the larger cutting forces, higher vibration levels, and thermal effects associated with higher cutting parameters in the machining process, all of which contribute to increased geometric distortions [51].

Recent results on the dry turning of A97075 [52] indicate that macrogeometric accuracy is strongly governed by cutting conditions, with feed emerging as a primary driver of

form errors, such as circular runout and straightness. This is consistent with the higher *RON* values obtained under the aggressive turning parameters, where increased mechanical loading and dynamic effects are expected to amplify deviation from the ideal circular profile.

When the specimens were exposed to corrosion (Fig. 7a), a moderate increase in *RON* was observed. The rise in form error is attributed to the development of pitting corrosion, which creates local cavities that disrupt the circular profile of the calibrated section. In some cases, the corrosion process led to higher localised deviations, reflecting the heterogeneous distribution of pits on the surface. These results indicate that corrosion consistently worsens the accuracy of roundness, although the extent of deterioration depends on the initial surface condition. This scatter is consistent with the stochastic nature of pitting in high-strength aluminium alloys, where the size and spatial distribution of the pit population are heterogeneous [53]. Under such conditions, localised cavities can dominate form descriptors; therefore, the same exposure may yield different levels of RON degradation depending on the most severe pits present in the calibrated section.

The effect of AJM strongly depended on whether it was applied before or after corrosion. When AJM was applied directly after machining (Fig. 7b), the roundness deviation increased regardless of the cutting conditions applied in the turning process. The abrasive particles eroded preferentially around existing irregularities, increasing the geometric error of smoother surfaces but having little impact when the deviations were already high. When corrosion followed AJM, the values remained high. This indicates that AJM produced additional irregularities that later acted as preferential nucleation sites for pitting corrosion, amplifying the effect of the environment and leading to unstable roundness values.

In contrast, the trend was reversed when AJM was applied after corrosion (Fig. 7a). Corrosion first increased the roundness under low and high cutting conditions, reflecting the pit-induced degradation. However, subsequent AJM treatment reduced these deviations, lowering the mean *RON* value. This indicates that AJM was capable of partially levelling the corrosion-induced defects, recovering part of the initial roundness accuracy.

A direct comparison of the two sequences reveals the decisive influence of the process order. When AJM was performed before corrosion, the abrasive action introduced additional irregularities that intensified the effect of corrosion, resulting in higher and less stable *RON* values. Conversely, the abrasive process acted beneficially when AJM was applied after corrosion, removing or smoothing corrosion pits and improving roundness. Therefore, the experimental results demonstrate that AJM is an effective corrective treatment when applied after corrosion, whereas its application before corrosion amplifies geometric deterioration.

A quantitative comparison of the final *RON* values confirms that the *RON* is also influenced by the postprocessing order. Under the low cutting parameter condition, the final *RON* increases from 6.07 µm when corrosion occurs before AJM to 7.92 µm with corrosion after AJM, corresponding to an increase of 30.5%. Under the high cutting-parameter condition, the final *RON* increased from 8.01 µm to 9.23 µm, corresponding to an increase of 15.2%. This result indicates that the sequencing of corrosion and AJM has a pronounced influence on the final *RON* values, which is consistent with the behaviour observed for *Ra* and *Rz*.

Under the lower feed rate, the measured STR values were markedly lower than those obtained under the aggressive cutting condition, confirming that higher v_c and f promote larger axial distortions along the generatrix of the calibrated section. This result is consistent with the greater mechanical loading, higher thermal input and increased vibration levels associated with severe cutting.

When corrosion preceded AJM (Fig. 8a), the first step substantially degraded the straightness relative to the *STR*

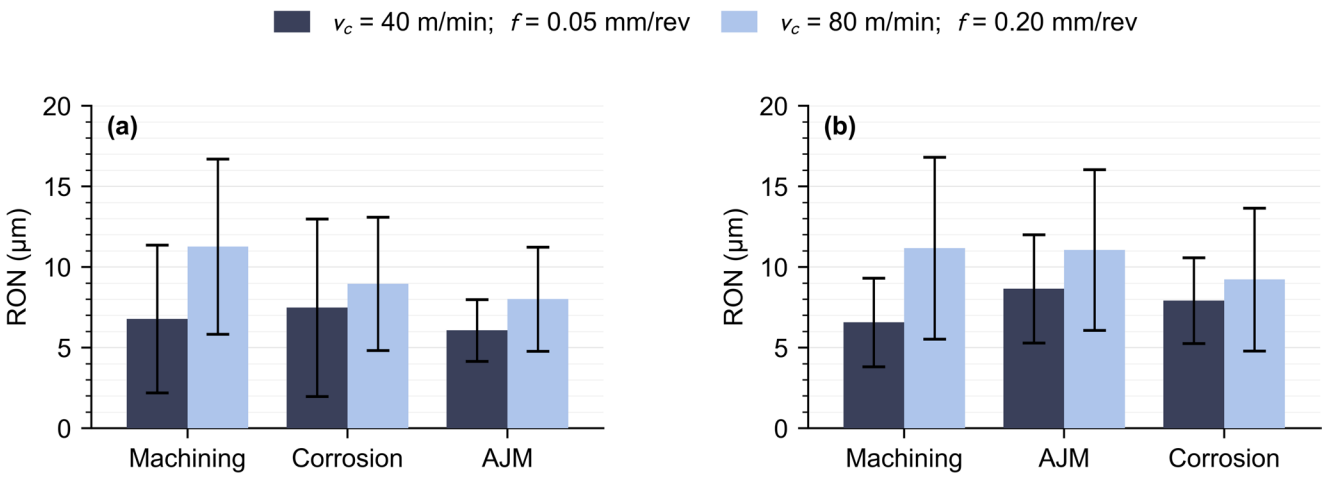

Fig. 7 Mean roundness values. (**a**) Corrosion before the AJM process; (**b**) AJM before corrosion

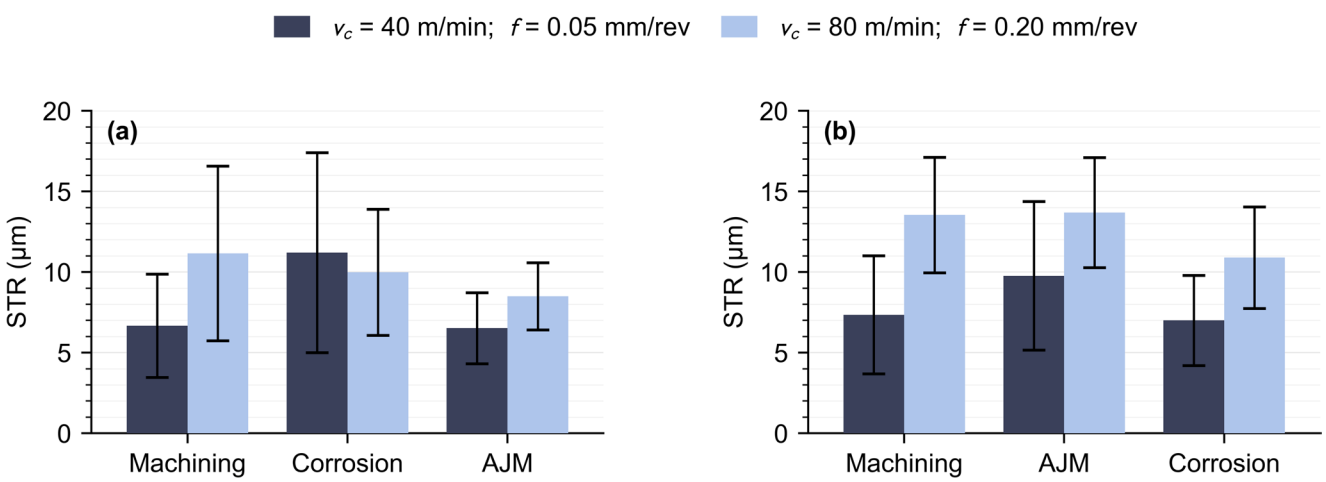

Fig. 8 The mean straightness values. (**a**) Corrosion before the AJM process; (**b**) AJM before the corrosion process

values obtained in the machined specimens. This is consistent with the formation of pits and cavities that modify the axial profile along the calibrated zone. The mean value decreased for aggressively machined specimens, implying that corrosion eroded axial peaks and smoothed long-wavelength features, thereby slightly reducing the measured deviation. After the subsequent AJM step, this process acted as a corrective treatment in both machining conditions, with its effect being more noticeable for low cutting parameter values. Therefore, corrosion introduced large anisotropic spikes, whereas the subsequent AJM pass reduced these extremes and homogenised the axial profile.

When AJM was applied directly after machining (Fig. 8b), *STR* increased in the conservatively machined specimens, indicating that the abrasive action introduced long-wavelength irregularities into profiles that were initially more linear. The mean value remained at a similar level in the aggressively machined specimens, suggesting that AJM offered little corrective effect when the axial form error was already high. After corrosion, *STR* decreased, despite the presence of some scattered high local values. This suggests that the corrosive attack generated heterogeneous pits while also removing or redistributing material at axial ridges, particularly in the aggressively machined specimens, thereby reducing the measured *STR* deviation.

Overall, the results demonstrate a strong order effect. Applying AJM before corrosion worsened *STR* in initially smooth specimens and created conditions favourable to anisotropic and irregular corrosion damage. Although a partial reduction in *STR* could be observed after corrosive exposure, the final *STR* remained comparatively high, especially under the more severe cutting parameters. In contrast, when corrosion preceded AJM, this sequence was consistently more favourable because corrosion first degraded the axial form and AJM then removed corrosion-induced defects, delivering the lowest final *STR* values across both machining conditions. AJM was therefore beneficial only when applied after corrosion, where it acted as a restorative operation.

The final straightness values also reflect the influence of the postprocessing order. The straightness deviation measured at the end of the sequence is higher when corrosion is carried out after AJM than when AJM is applied after corrosion. For the low cutting parameter condition, the final *STR* increases from 6.52 µm to 7.00 µm, which corresponds to an increase of 7.4%. For the high cutting parameter condition, the final *STR* increases from 8.50 µm to 10.90 µm, corresponding to an increase of 28.2%. Overall, sequencing produces a consistent and measurable shift in *STR* across both machining conditions.

The cylindricity deviation (*CYL*) measured after machining (Fig. 9) showed moderate values that reflected the combined contributions of roundness and straightness errors. The average *CYL* under the lower cutting parameters was of the same order as that measured under the higher cutting parameters. These results confirm that cylindricity is highly sensitive to local tool–workpiece interaction, vibration and thermal effects during turning. Although higher form errors are generally expected under aggressive cutting conditions, the observed dispersion indicates that local variations in cutting dynamics can sometimes have a stronger influence than v_c and f alone.

The corroded specimens after machining (Fig. 9a) showed the most severe impact on *CYL*. This behaviour reflects the disruptive effect of deep pits and localised cavities, which distort the cylindrical profile across the length of the evaluation. The results indicate that the cutting parameters did not significantly affect the *CYL* values after corrosion because the initial pre-corrosion condition was already similar in both conditions.

However, the subsequent AJM step reduced the average deviation. Although these values are still significantly

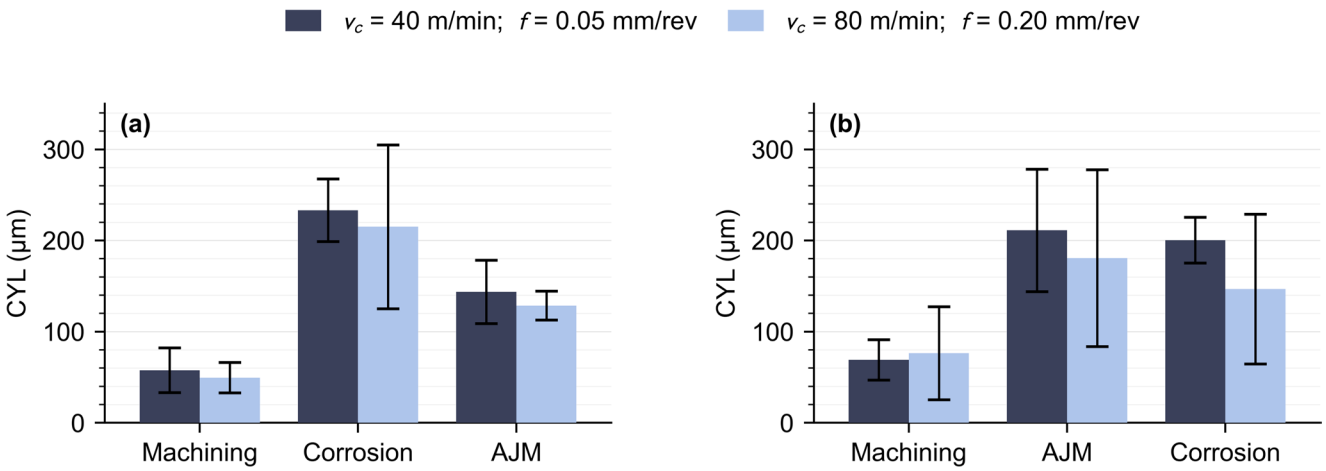

Fig. 9 Mean cylindricity values (**a**) Corrosion before the AJM process; (**b**) AJM before the corrosion process

higher than those of the machined process, they represent a substantial recovery relative to the corroded state, confirming that AJM can remove corrosion-induced irregularities and partially level the cylindrical profile.

When AJM was applied directly after machining (Fig. 9b), a pronounced degradation of cylindricity was observed in both machining conditions. This deterioration is explained by the fact that the abrasive jet produces long-wavelength distortions and accentuates axial irregularities, amplifying deviations from the ideal cylindrical geometry. Following subsequent corrosion, a slight reduction in *CYL* was observed. This partial recovery is linked to the preferential corrosion of material peaks introduced by AJM, which can smooth certain protrusions. Nevertheless, the final values remained well above the initial machined condition, indicating that this sequence is strongly harmful to the preservation of cylindrical accuracy.

The observed sensitivity of *RON* and the analogous behaviour found for *STR* and *CYL* are also consistent with recent studies on jet-based abrasive processing [54], where circularity and cylindricity respond to jet conditions and abrasive delivery through changes in material removal distribution. This supports the interpretation that the AJM step can either aggravate macrogeometric errors when applied to initially regular surfaces or partially restore geometric integrity by removing part of the corrosion-induced irregularities when applied after corrosion.

These results demonstrate that AJM can be beneficial only when applied after corrosion, functioning as a restorative operation. If applied before corrosion, AJM amplifies the susceptibility of the surface to further degradation and yields the worst cylindricity outcomes. In addition, it can be considered that *CYL* is the most sensitive of the form parameters evaluated, showing deviations an order of magnitude larger than roundness or straightness.

This sensitivity is also reflected in the cylindricity outcomes when the two sequences are contrasted. When corrosion is carried out after AJM, the final *CYL* deviation remains higher than in the case where AJM is applied after corrosion. Under the low cutting-parameter condition, the final *CYL* increased from 143.63 µm to 200.35 µm, which corresponds to an increase of 39.5%. Under the high cutting-parameter condition, the final *CYL* increased from 128.55 µm to 146.74 µm, corresponding to an increase of 14.1%. In practical terms, these results show that the order of corrosion and AJM systematically shifts the final cylindricity, reinforcing the sequencing effect observed in roughness and other form descriptors.

3.3 Fatigue behaviour analysis

The fatigue behaviour of the tested specimens clearly depended on both the machining parameters and the post-processing operation sequence (Fig. 10). A certain scatter in fatigue life is observed across all conditions, as reflected by the error bars in Fig. 10. This behaviour is expected in corrosion-affected and surface-modified specimens, where crack initiation is governed by the local severity and spatial distribution of surface defects and corrosion pits, as well as by the surface changes induced by AJM. Despite this inherent variability, the comparative trend between the two sequencing routes remains consistent, and all tests ended in complete fracture within the calibrated section.

Under low cutting parameters (v_c = 40 m/min; f=0.05 mm/rev), corrosion before the AJM sequence did not critically compromise mechanical endurance, and the final condition retained a moderate resistance to fatigue loading. In contrast, when the sequence was reversed and AJM was applied before corrosion, the mean fatigue life substantially decreased, corresponding to a reduction of approximately

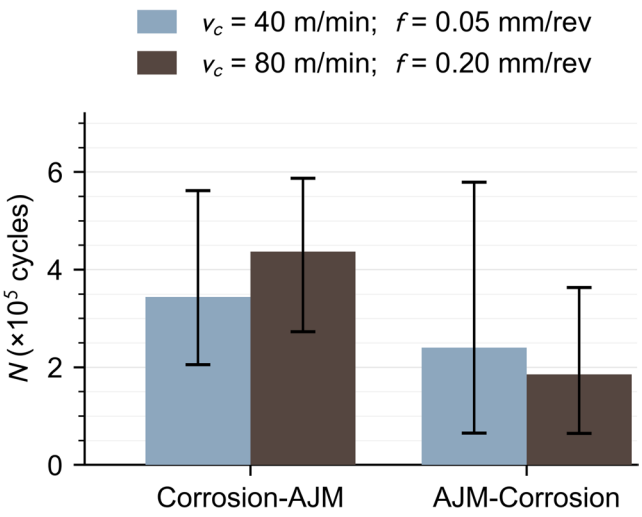

Fig. 10 Number of fatigue test cycles

30%. This behaviour indicates that applying AJM before corrosion can markedly reduce fatigue resistance because the abrasive process introduces surface irregularities that act as stress raisers and interact with subsequent pitting, accelerating crack initiation.

For specimens machined under higher cutting parameters (v_c = 80 m/min; f=0.20 mm/rev), the same trend was observed, although the differences were even more pronounced. When AJM was applied after corrosion, the highest fatigue life of all conditions was obtained, which is particularly notable given the poor initial surface state associated with the aggressive cutting parameters. This suggests that the corrective effect of AJM after corrosion at least partly mitigated the harmful influence of machining and corrosive attack. By contrast, when corrosion was applied after AJM, the shortest fatigue life was recorded, with a reduction of more than 55% compared with the corrosion before AJM sequence under the same cutting parameters. The combination of high initial roughness, large form deviations and subsequent pitting under this sequence created highly favourable conditions for premature crack initiation and propagation.

When the four cases are compared, the sequencing of postprocessing operations exerts a stronger influence on fatigue resistance than the machining parameters. Notably, the sequence that yields higher final roughness and larger form deviations, particularly cylindricity, is also associated with lower fatigue lives. This qualitative consistency supports the interpretation that the postprocessing order influences fatigue performance through its effect on surface integrity, combining corrosion-induced local defects with macroform changes. While a direct causal attribution to any single descriptor is outside the scope of the present dataset, the observed trends are consistent across roughness, form metrics, and fatigue outcomes. This demonstrates that the order in which surface treatments are applied can offset or aggravate the initial state left by machining.

Beyond the roughness and macro-form descriptors, the difference between sequences can be rationalised by the evolution of local corrosion-related defects that control crack initiation. When corrosion is applied first, pitting acts as a surface notch. Subsequent application of AJM can partially remove corrosion products, damaged surface layers, and blunt pit edges, thereby reducing the effective notch severity at the pit mouth. Conversely, when AJM is applied before corrosion, the abrasive action can introduce surface irregularities and micro-notches that promote local electrolyte retention and preferential pit nucleation during subsequent exposure, leading to more severe stress raisers and earlier crack initiation. This interpretation is consistent with the measured trends in roughness, form deviations, and fatigue life under the investigated conditions.

The surface roughness trends further support this interpretation. After machining, the *Ra* values were relatively low, which is consistent with higher fatigue life. Corrosion increased roughness by introducing pits that acted as preferential crack nucleation sites. When AJM was applied after corrosion, the roughness remained comparatively stable, and the damaged surface layer was partially removed, thereby improving fatigue endurance. In contrast, when AJM preceded corrosion, the surface reached the highest roughness levels, promoting strong stress concentration and explaining the reduced fatigue lives.

The form deviation results reinforce this interpretation. *RON* and *STR* errors were consistently lower in the corrosion before AJM sequence, in which AJM acted as a corrective treatment by reducing the severity of pits and restoring axial regularity. Although cylindricity exhibited larger absolute deviations, it followed the same overall trend, with lower final values when AJM was applied after corrosion. By contrast, when AJM was performed before corrosion, both *RON* and *CYL* deteriorated markedly, amplifying the effect of subsequent pitting and generating anisotropic geometries that intensified stress concentration. Taken together, these findings show that the fatigue life of UNS A97075 aluminium depends not only on the initial machining conditions but also very strongly on the sequence in which the postprocessing operations are applied.

The abovementioned fatigue trends are consistent with the mechanisms described for high-strength aluminium alloys affected by pitting corrosion and particle impact surface modification. Dey et al. [53] showed that pitting generates a heterogeneous defect population and that fatigue crack initiation is governed by the most severe pits, which provides a rationale for the observed scatter in corrosion-affected conditions and for the strong sensitivity of fatigue life to local defect severity. In addition, Dai et al. [39]

demonstrated in grit blasting that particle impacts produce craters and surface scratching that become preferential initiation features and can markedly reduce fatigue performance when they dominate the near-surface topography. In this framework, the lower lives measured when AJM precedes corrosion are consistent with the accumulation of impact-induced irregularities and subsequent pitting on an already notched surface, whereas the improved endurance obtained when AJM follows corrosion is consistent with a reduction in the effective severity of corrosion-related surface defects through partial removal of the damaged layer and redistribution of the extreme surface features.

From a sustainability perspective, dry turning reduces the environmental burden associated with cutting fluids, whereas adding an AJM step introduces additional energy demand and abrasive consumption. However, when AJM is applied after corrosion as a corrective operation and helps to recover fatigue life, it may extend component life and reduce the need for replacement and remanufacturing.

4 Discussion

The previous sections described the evolution of surface roughness, geometric deviations and fatigue performance under different process sequences. This section integrates those variables in order to clarify the mechanisms governing fatigue behaviour in UNS A97075. By analysing the interaction between local defect severity, global geometric integrity and process order, a broader understanding can be developed of how surface integrity evolves throughout the manufacturing and maintenance stages.

The evolution of surface integrity throughout the different processing stages plays a central role in defining the fatigue response of UNS A97075. Although *Ra* provides a general description of surface quality, the most severe local defect present within the highly stressed region typically governs fatigue crack initiation [39, 53]. Therefore, the effective defect severity, rather than the mean surface condition, must be considered when interpreting the observed trends in fatigue life.

After machining, the surface is characterised by regular feed marks and a relatively homogeneous topography. Under these conditions, crack initiation is governed mainly by the geometrical features associated with the cutting process, such as groove depth and residual stress distribution. When corrosion is introduced, the surface state changes fundamentally. Localised pitting creates cavities of variable depth and morphology, generating sharp stress concentrators that dominate crack initiation [31, 32]. At this stage, parameters that are sensitive to extreme profile variations, such as *Rz*, become more representative of the fatigue-controlling features than average parameters such as *Ra*.

The application of the AJM process modifies this defect population in different ways depending on the initial surface condition. When applied to a corroded surface, the abrasive action can partially remove corrosion products and smooth the edges of pits, thereby reducing the effective stress concentration at the pit mouth [53, 55]. In contrast, particle impacts introduce additional surface irregularities and microindentations when applied to a surface that has not yet been exposed to corrosion. These features may act as preferential sites for electrolyte retention and subsequent pit nucleation, leading to a more severe defect population after corrosion exposure [37, 56].

Therefore, fatigue behaviour is governed not simply by the magnitude of roughness or by the presence of corrosion alone, but by the evolution of the most critical surface defects along the process chain. The experimental results suggest that fatigue life is controlled by the interaction between pit geometry, impact-induced irregularities and the modification of defect sharpness during abrasive treatment. Under the conditions investigated, the most favourable sequence was corrosion followed by AJM, because corrosion first defined the dominant defect population and the subsequent abrasive treatment then removed corrosion products and reduced the effective severity of the pits by modifying their surface geometry. By contrast, when AJM preceded corrosion, the impact features introduced at the surface promoted localised pit nucleation during subsequent exposure, leading to a more severe defect population and earlier crack initiation. This indicates that AJM is better suited to post-corrosion reconditioning step in aerospace manufacturing and maintenance chains than as a preventive pre-exposure treatment when the aim is to preserve fatigue performance.

The macrogeometric deviations RON, *STR*, and *CYL* describe global geometric imperfections that may alter the nominal stress field and modify the local stress amplitude experienced at specific surface locations. Although these deviations are typically smaller in magnitude than corrosion pits, their influence lies in their ability to redistribute stresses along the specimen surface [51].

The experimental results indicate that macrogeometric parameters alone do not fully determine fatigue performance. Instead, their role appears to be synergistic. When severe pits or impact-induced irregularities are present, macrogeometric deviations amplify their effect by increasing the local stress acting at the most critical defect. Conversely, when the surface defect population is less severe, variations in RON or CYL have a more limited influence on fatigue life.

This interaction helps explain why the improvements in geometric accuracy observed when AJM is applied after corrosion are accompanied by enhanced fatigue behaviour. In this scenario, the abrasive process modifies local surface defects and partially restores global geometric regularity, consistent with a reduction in the effective stress concentration within the calibrated section. In contrast, when abrasive treatment precedes corrosion, the combined presence of macrogeometric distortions and newly formed pits is associated with higher fatigue damage, suggesting a compounded stress concentration effect that accelerates crack initiation.

Therefore, in the present study, fatigue performance should be interpreted as the outcome of a coupled interaction between local defect severity and global geometric integrity. Neither microgeometric roughness nor macrogeometric deviations act independently; rather, their combined evolution along the processing sequence determines the effective stress concentration that controls crack initiation.

Within the investigated conditions, the results suggest a clear hierarchy of influence on fatigue behaviour. First, the dominant factor is the sequence in which corrosion and AJM are applied, because this determines the final severity of the surface defect population. Second, the local defect severity associated with pits, impact marks, and their resulting geometry governs crack initiation more directly than the average surface condition. Third, macrogeometric deviations such as roundness, straightness, and cylindricity modulate the local stress distribution and can amplify the effect of the most critical defects. Finally, the initial turning condition remains relevant because it defines the starting surface state, but its influence becomes secondary once corrosion and AJM modify the surface through the subsequent stages. This hierarchy explains why the same turning condition can lead to markedly different fatigue responses depending on the postprocessing route.

This hierarchy is consistent with the experimental results, which show that the corrosion and AJM sequence exerts a stronger influence on fatigue performance than the initial turning parameters. Although the initial surface condition is modified by variations in cutting speed and feed, their effect becomes secondary once the surface is subjected to corrosion and abrasive treatment. This indicates that the interaction between these subsequent processes primarily defines the final defect population responsible for crack initiation.

When AJM is applied after corrosion, the abrasive action interacts with a surface already containing pits and corrosion products. Under these conditions, the process removes loose oxide layers, reduces the sharpness of pit edges, and partially levels the most critical surface irregularities. Although still affected by prior corrosion, the resulting surface state presents a reduced effective defect severity. Consequently, crack initiation is delayed, and fatigue life increases.

By contrast, when AJM precedes corrosion, the surface already contains impact-induced irregularities and micro-indentations at the moment of exposure to the aggressive environment. These features modify the local surface energy and topography, creating favourable conditions for localised electrolyte retention and pit nucleation. The subsequent corrosion process therefore develops on a surface that is already geometrically disturbed, leading to a more heterogeneous and severe defect population. The combined presence of impact features and corrosion accelerates crack initiation and reduces fatigue life.

The fact that this antagonistic behaviour appears consistently under both machining conditions confirms that process sequencing governs the final structural response more strongly than the initial cutting parameters. This means that surface treatments cannot be evaluated independently from the environmental exposure stage. The fatigue performance of the component is determined by the cumulative development of surface defects throughout the manufacturing or maintenance sequence rather than a single operation.

This finding has important implications for surface engineering strategies in aerospace aluminium alloys. It suggests that AJM should be considered primarily as a corrective treatment after corrosion damage rather than as a preventive treatment before environmental exposure, at least under the processing conditions investigated in this study.

In manufacturing scenarios, AJM may be considered a post-machining finishing operation intended to modify the surface texture or improve the geometric accuracy before the component enters service. However, the present findings indicate that if such treatment is followed by environmental exposure, the altered surface topography may influence subsequent corrosion development and ultimately reduce fatigue performance.

In maintenance or repair contexts, abrasive treatments are frequently employed to remove oxide layers, corrosion products, or superficial damage. The present results suggest that AJM can partially reduce defect severity and improve the geometric regularity of the component when applied after corrosion has developed, thereby supporting fatigue life recovery. This highlights the importance of evaluating the surface condition before treatment and selecting the appropriate process sequence.

More broadly, the study demonstrates that surface integrity should be considered an evolving state rather than the outcome of a single manufacturing step. The final fatigue behaviour emerges from the cumulative interaction among machining, environmental degradation, and surface modification processes. Therefore, optimisation strategies for aerospace aluminium alloys should focus on controlling the sequence and interaction of processes throughout the component life cycle rather than focusing exclusively on improving individual operations.

The mechanistic interpretation proposed in this study is supported by consistent trends in roughness, form deviations, and fatigue life across the investigated process sequences. However, the present work does not include direct fractographic examination, residual stress measurements, or subsurface microstructural characterisation after turning, corrosion, and AJM. For this reason, the proposed explanation should be understood as a physically supported interpretation derived from the measured surface integrity and fatigue results, rather than as a direct microstructural verification of the crack initiation mechanism. Future work should therefore combine the present macroscopic and functional approach with direct characterisation of pits, impact features, and fracture initiation zones.

5 Conclusions

This study provides a comprehensive assessment of how machining parameters, corrosion and Abrasive Jet Machining (AJM) interact to define the surface integrity and fatigue performance of UNS A97075 aluminium alloy. By integrating macrogeometric form deviations, namely roundness, straightness and cylindricity, with microgeometric roughness parameters (*Ra* and *Rz*) and fatigue behaviour, the work offers a multiscale perspective that strengthens understanding of surface–process interactions in aeronautical components.

From a macrogeometric standpoint, roundness, straightness and cylindricity were highly sensitive to the combined action of corrosion and AJM. Corrosion consistently degraded form accuracy through pit formation and cavity development. By contrast, AJM showed a strongly sequence-dependent response. When corrosion followed AJM, the final surface condition deteriorated markedly, and the final cylindricity deviation increased by approximately 14% to 40%, confirming that this order amplifies geometric deterioration. Under the same sequence, the final roughness increased by approximately 49% to 91% in *Ra* and 66% to 78% in *Rz* relative to the sequence in which AJM was applied after corrosion. Conversely, when AJM was applied after corrosion, it acted as a corrective post-treatment and partially restored cylindrical regularity by mitigating corrosion-induced surface damage. This asymmetry highlights the decisive role of process order. AJM should therefore be regarded as primarily restorative when used after corrosion, whereas its application before corrosion entails a greater risk of degrading surface integrity.

These conclusions apply to the AJM conditions adopted in this study and to corrosion damage dominated by pitting-type surface defects comparable to the exposure examined in this study. Different AJM parameter settings, particularly milder regimes or alternative abrasive characteristics, may modify the severity of surface alterations and the subsequent corrosion and fatigue response. In scenarios involving severe corrosion with significant material loss or deeper defects, a case-specific inspection and validation should be performed before applying AJM as a corrective operation. A complementary assessment of possible subsurface alterations induced by turning and AJM would further refine the mechanistic interpretation and is a topic for future investigation.

On the microgeometric scale, roughness evolved in the same antagonistic manner. Corrosion increased surface irregularity, but AJM applied afterwards could smooth some corrosion-induced defects, whereas the reverse sequence intensified damage. Taken together, the roughness and form-deviation results support the interpretation that surface quality is not the intrinsic outcome of a single operation, but rather the cumulative result of sequential processes.

Fatigue life measurements confirmed that the synergy between surface roughness, form errors, and corrosion defects determines crack initiation and propagation. Specimens subjected to corrosion before the AJM sequence exhibited the longest endurance, even under severe cutting conditions, highlighting the capacity of AJM to partially compensate for poor initial machining and corrosive damage. Conversely, the AJM before corrosion sequence resulted in the shortest fatigue life, reflecting the harmful synergy of abrasive-induced irregularities with subsequent pitting. These findings show that surface treatments can either mitigate or aggravate the intrinsic weaknesses of machining, depending on the sequence of application.

This work contributes to both the scientific understanding of surface process interactions and the practical definition of manufacturing and repair strategies for aluminium alloy components operating in aggressive environments. Within the investigated conditions, fatigue performance was governed more strongly by the sequence of corrosion and AJM than by the initial turning parameters. This identifies process order as a critical variable in the design of post machining and maintenance routes for UNS A97075 components exposed to corrosive environments. Ultimately, the results show that preserving structural reliability requires controlling not only the quality of each individual operation, but also the order in which surface modification and environmental exposure take place.

Acknowledgements The authors thank the University of Malaga-Andalucía Tech Campus for its contribution to this work.

Author Contributions Conceptualisation, S.M.B. and F.J.T.V.; methodology, S.M.B. and M.H.F.; formal analysis, S.M.B., I.R.L. and F.J.T.V.; investigation, S.M.B. and F.J.T.V.; data curation, S.M.B., I.R.L. and F.J.T.V.; writing, S.M.B.; supervision, F.J.T.V. and L.S.H.; project administration, M.H.F., S.M.B., F.J.T.V. and L.S.H.

Funding Funding for open access publishing: Universidad de Málaga/CBUA. This work received funding from the Ministry of Science and Innovation (Government of Spain), the State Research Agency and by FEDER through the research project 'Expert system for improving surface integrity in sustainable machining of light alloys (SPAREMETAL),'' with reference PID2021-125988OB-I00.

Data availability The datasets generated are available from the corresponding author on reasonable request.

Code Availability Not applicable.

Declarations

Conflict of interest The authors declare no conflicts of interest.

References

1. Gloeckner P, Rodway C (2017) The evolution of reliability and efficiency of aerospace bearing systems. Engineering 09(11):962–991. https://doi.org/10.4236/eng.2017.911058
2. Vartanov G (2021) High strength corrosion resistant steel for aircraft landing gears and structures. SAE Int J Adv Curr Pract Mobil 3(3):2021-01–0028. https://doi.org/10.4271/2021-01-0028
3. Singh J, Srivastawa K, Jana S, Dixit C, S R (2024) Advancements in lightweight materials for aerospace structures: A comprehensive review. Acceleron Aerospace Journal 2(3):173–183. https://doi.org/10.61359/11.2106-2409
4. Martínez-Viademonte MP, Abrahami ST, Hack T, Burchardt M, Terryn H (2020) A review on anodizing of aerospace aluminum alloys for corrosion protection. Coatings 10(11):1106. https://doi.org/10.3390/coatings10111106
5. Li S et al (2023) Development and applications of aluminum alloys for aerospace industry. J Mater Res Technol 27:944–983. https://doi.org/10.1016/j.jmrt.2023.09.274
6. Maruthuvakudi Venkatram N, Alsabeeha S, Weston NR, Liu Z, Mavris DN (2024) Life Cycle Assessment and Risk Evaluation of CFRP in Aerospace. in AIAA SCITECH 2024 Forum. American Institute of Aeronautics and Astronautics, Reston, Virginia. doi: https://doi.org/10.2514/6.2024-1217.
7. Ben Moses R, Raj RA, Judges IV, Srinivas PB (2024) Casting and microstructural characterization of high-performance 2000 series aluminum alloy for aerospace applications. J Phys Conf Ser 2837(1):012103. https://doi.org/10.1088/1742-6596/2837/1/012103
8. Fernandez-Vidal SR, Fernandez-Vidal S, Batista M, Salguero J (2018) Tool wear mechanism in cutting of stack CFRP/UNS A97075. Materials. https://doi.org/10.3390/ma11081276
9. Abdellah MY (2021) Ductile fracture and S–N curve simulation of a 7075-T6 aluminum alloy under static and constant low-cycle fatigue. J Fail Anal Prev 21(4):1476–1488. https://doi.org/10.1007/s11668-021-01202-x
10. Dursun T, Soutis C (2014) Recent developments in advanced aircraft aluminium alloys. Materials & Design (1980–2015) 56:862–871. https://doi.org/10.1016/j.matdes.2013.12.002
11. Rambabu P, Eswara Prasad N, Kutumbarao VV, Wanhill RJH (2017) Aluminium Alloys for Aerospace Applications. pp 29–52. https://doi.org/10.1007/978-981-10-2134-3_2
12. Bañon F, Sambruno A, Batista M, Simonet B, Salguero J (2020) Surface quality and free energy evaluation of s275 steel by shot blasting, abrasive water jet texturing and laser surface texturing. Metals. https://doi.org/10.3390/met10020290
13. Vazquez-Martinez JM, Gomez JS, Ares PFM, Fernandez-Vidal SR, Ponce MB (2018) Effects of laser microtexturing on the wetting behavior of Ti6Al4V alloy. Coatings 8(4):145. https://doi.org/10.3390/COATINGS8040145
14. Liao Z et al (2021) Surface integrity in metal machining - Part I: Fundamentals of surface characteristics and formation mechanisms. Int J Mach Tools Manuf 162:103687. https://doi.org/10.1016/j.ijmachtools.2020.103687
15. Béjar SM, Vilches FJT, Gamboa CB, Hurtado LS (2019) Parametric analysis of macro-geometrical deviations in dry turning of UNS A97075 (Al-Zn) alloy. Metals. https://doi.org/10.3390/met9111141
16. Rotella G (2019) Effect of surface integrity induced by machining on high cycle fatigue life of 7075-T6 aluminum alloy. J Manuf Process 41:83–91. https://doi.org/10.1016/j.jmapro.2019.03.031
17. De Agustina B, Rubio EM, Sebastián MÁ (2012) Surface roughness predictive model of UNS A97075 aluminum pieces obtained by dry turning tests based on the cutting forces. Appl Mech Mater 1628–1635. https://doi.org/10.4028/www.scientific.net/AMM.217-219.1628
18. Vié T, Godin N, Deschanel S, Normand B (2023) On the effect of coatings and pre-corrosion during fatigue tests of 7075-T6 aluminum alloy monitored with acoustic emission (AE). E-J Nondestructive Test 28(1). https://doi.org/10.58286/27629
19. Şahinoğlu A, Karabulut Ş, Güllü A (2017) Study on spindle vibration and surface finish in turning of Al 7075. Solid State Phenom 261:321–327. https://doi.org/10.4028/www.scientific.net/SSP.261.321
20. Du F, He L, Huang H, Zhou T, Wu J (2020) Analysis and multi-objective optimization for reducing energy consumption and improving surface quality during dry machining of 304 Stainless Steel. Materials 13(21):4693. https://doi.org/10.3390/ma13214693
21. Sharma AK, Tiwari AK, Dixit AR (2016) Effects of Minimum Quantity Lubrication (MQL) in machining processes using conventional and nanofluid based cutting fluids: A comprehensive review. J Clean Prod 127:1–18. https://doi.org/10.1016/j.jclepro.2016.03.146
22. Pusavec F, Krajnik P, Kopac J (2010) Transitioning to sustainable production – Part I: Application on machining technologies. J Clean Prod 18(2):174–184. https://doi.org/10.1016/j.jclepro.2009.08.010
23. Rodriguez I, Arrazola PJ, Cuesta M, Sterle L, Pušavec F (2023) Improving surface integrity when drilling CFRPs and Ti-6Al-4V using sustainable lubricated liquid carbon dioxide. Chin J Aeronaut 36(7):129–146. https://doi.org/10.1016/j.cja.2022.09.004
24. Saranu R, Chanamala R, Putti SR (2020) Processing, micro structures and mechanical properties of AZ91E, Sic and fly ash composites: a review. Mater Today Proc 26:2629–2635. https://doi.org/10.1016/j.matpr.2020.02.555
25. Takenaka K et al (2022) Development of a non-thermal atmospheric pressure plasma-assisted technology for the direct joining

of metals with dissimilar materials. J Manuf Process 75:664–669. https://doi.org/10.1016/j.jmapro.2022.01.041
26. Kwon D-K, Lee J-H (2022) Performance improvement of micro-abrasive jet blasting process for Al 6061. Processes 10(11):2247. https://doi.org/10.3390/pr10112247
27. Gajera VM, Swarrop C (2011) Process modeling and simulation of abrasive jet machine-a review. Indian J Appl Res 4(6):1–3. https://doi.org/10.15373/2249555X/June2014/186
28. Lv Z, Hou R, Wang R, Zhang Y, Zhang M (2022) Numerical investigation on the residual stress in abrasive waterjet peening. Int J Adv Manuf Technol 123(5–6):1695–1706. https://doi.org/10.1007/s00170-022-10285-1
29. Pramanik A et al (2017) Fatigue life of machined components. Adv Manuf 5(1):59–76. https://doi.org/10.1007/s40436-016-0168-z
30. Zhuang K et al (2025) Surface modification of titanium alloy using a novel elastic abrasive jet machining method. Surf Coat Technol 495:131573. https://doi.org/10.1016/j.surfcoat.2024.131573
31. Fujii T, Ito D, Shimamura Y (2023) Growth characteristics of stress corrosion cracking in high-strength 7075 aluminum alloy in sodium chloride solutions. Eng Fract Mech 292:109657. https://doi.org/10.1016/j.engfracmech.2023.109657
32. Shi L, Xiang L, Tao J, Chen Q, Liu J, Zhong Y (2022) Actual marine atmospheric pre-corrosion fatigue performance of 7075-T73 aluminum alloy. Metals Basel 12(5):874. https://doi.org/10.3390/met12050874
33. Gomes RC, Araújo JA, Cardoso RA, Ferreira JLA, Silva CRM (2023) Fatigue life prediction using critical distance on aluminum alloy wire containing indentation produced marks. Theor Appl Fract Mech 128:104135. https://doi.org/10.1016/j.tafmec.2023.104135
34. Xu X, Liu D, Zhang X, Liu C, Liu D (2020) Mechanical and corrosion fatigue behaviors of gradient structured 7B50-T7751 aluminum alloy processed via ultrasonic surface rolling. J Mater Sci Technol 40:88–98. https://doi.org/10.1016/j.jmst.2019.08.030
35. Béjar SM, Vilches FJT, Gamboa CB, Hurtado LS (2020) Fatigue behavior parametric analysis of dry machined uns a97075 aluminum alloy. Met (Basel) 10(5). https://doi.org/10.3390/met10050631
36. Berry L, Wheatley G, Ma W, Masoudi Nejad R, Berto F (2022) The influence of milling induced residual stress on fatigue life of aluminum alloys. Forces in Mechanics 7:100096. https://doi.org/10.1016/j.finmec.2022.100096
37. Song H, Liu J, Zhang H, Du J (2023) Multi-source data driven fatigue failure analysis and life prediction of pre-corroded aluminum–lithium alloy 2050-T8. Eng Fract Mech 292:109626. https://doi.org/10.1016/j.engfracmech.2023.109626
38. Vinay S, Bhanwal S, Yadav S (2021) Abrasive jet machining and optimization of process parameters. Int. J. Adv. Res. (Indore) 9(5):607–616. https://doi.org/10.21474/IJAR01/12883
39. Dai W et al (2024) Effect of grit blasting on fatigue behavior of 2024-T3 aero Al alloy,. J Mater Res Technol 32:519–529. https://doi.org/10.1016/j.jmrt.2024.07.184
40. Bakir A et al (2025) Fatigue performance of cold spray repaired aluminium alloy 7075,. Int J Fatigue 198:109036. https://doi.org/10.1016/j.ijfatigue.2025.109036
41. Sarkar A, Tråstadkjølen SU, Wilson H, Holmestad J, Nyhus B, Razavi N (2025) Influence of prior corrosion on fatigue behaviour in a simulated recycled 6082 Al-alloy,. Materialia 44:102556. https://doi.org/10.1016/j.mtla.2025.102556
42. Organization IS (2010) ISO 1143:2010. Metallic materials — Rotating bar bending fatigue testing, Geneva, Switzerland
43. Mohamad N, Ariffin MKAM, Mustapha F, bin Baharudin BTHT (2023) Challenges in machining composite materials: impact of machining parameters on cutting force,. Int J Mod Manuf Technol 15(3):98–106. https://doi.org/10.54684/ijmmt.2023.15.3.98
44. Zhu Y et al (2022) Surface formation mechanics and its microstructural characteristics of AAJP of aluminum alloy by using amino thermosetting plastic abrasive,. Int J Precis Eng Manuf Green Technol 9(1):59–72. https://doi.org/10.1007/s40684-020-00284-6
45. Organization IS ISO 4288:1998. Geometrical product specifications (GPS) - Surface texture: Profile method - Rules and procedures for the assessment of surface texture, 1998, *Geneva, Switzerland*
46. Macek W, Rozumek D, Faszynka S, Branco R, Zhu S-P, Masoudi Nejad R (2023) Fractographic-fractal dimension correlation with crack initiation and fatigue life for notched aluminium alloys under bending load,. Eng Fail Anal 149:107285. https://doi.org/10.1016/j.engfailanal.2023.107285
47. Organization IS (2011) ISO 12181-1:2011, Geometrical Product Specifications (GPS)–Roundness– Part 1: Terms, Definitions and Parameters of Roundness, Geneva, Switzerland
48. Organization IS (2011) ISO 12780-1:2011, Geometrical product specifications (GPS) — Straightness — Part 1: Vocabulary and parameters of straightness, Geneva, Switzerland
49. Zdravković N et al (2024) Influence of surface preparation of aluminum alloy AW-5754 and stainless steel X5CRNI18-10 on the properties of bonded joints,. Materials 17(11):2561. https://doi.org/10.3390/ma17112561
50. Campos-Jurado M, Rodríguez-Alabanda Ó, Guerrero-Vacas G (2025) Manufacturing of polymer–metal composite by fused filament fabrication: adhesion of PLA and PETG on aluminum,. Polymers 17(16):2210. https://doi.org/10.3390/polym17162210
51. Tangjitsitcharoen S, Chanthana D (2018) In-process prediction of roundness based on dynamic cutting forces,. Int J Adv Manuf Technol 94(5–8):2229–2238. https://doi.org/10.1007/s00170-017-1047-x
52. Trujillo FJ, Martín-Béjar S, Bañón F, Andersson T, Sevilla L (2025) Ann-based predictive model of geometrical deviations in dry turning of AA7075 (Al-Zn) alloy,. Measurement 243:116355. https://doi.org/10.1016/j.measurement.2024.116355
53. Dey S, Chattoraj I, Sivaprasad S (2025) Effect of pitting corrosion on fatigue life of T6 and T73 of 7075 aluminum alloy,. Int J Fatigue 200:109073. https://doi.org/10.1016/j.ijfatigue.2025.109073
54. Shi H, Giasin K, Barouni A, Zhang Z (2024) An experimental assessment and optimisation of hole quality in Al2024-T3 aluminium alloy during abrasive water jet machining,. Int J Adv Manuf Technol 130(11–12):5199–5218. https://doi.org/10.1007/s00170-024-13009-9
55. Sołtysiak R, Boroński D (2015) Strain analysis at notch root in laser welded samples using material properties of individual weld zones,. Int J Fatigue 74:71–80. https://doi.org/10.1016/j.ijfatigue.2014.12.004
56. Aung NN, Zhou W (2010) Effect of grain size and twins on corrosion behaviour of AZ31B magnesium alloy,. Corros Sci 52(2):589–594. https://doi.org/10.1016/j.corsci.2009.10.018